Modeling for periodic striation and microstructure evolution in active gas melt laser cutting for phase hardened parts

ARTICLE *in* INTERNATIONAL JOURNAL OF ADVANCED MANUFACTURING TECHNOLOGY · FEBRUARY 2014

Impact Factor: 1.78 · DOI: 10.1007/s00170-013-5385-z

4 AUTHORS, INCLUDING:

Peixing Liu
Huazhong University of Science and Techn…
5 PUBLICATIONS **2** CITATIONS
SEE PROFILE

Zhang Yisheng
Huazhong University of Science and Techn…
60 PUBLICATIONS **218** CITATIONS
SEE PROFILE

Zhong-xiang Gui
No.38 Research Institute,Chinese Electroni…
8 PUBLICATIONS **5** CITATIONS
SEE PROFILE

Int J Adv Manuf Technol (2014) 70:1421–1426
DOI 10.1007/s00170-013-5385-z

ORIGINAL ARTICLE

Modeling for periodic striation and microstructure evolution in active gas melt laser cutting for phase hardened parts

Peixing Liu · Yisheng Zhang · Huiqiang Liu · Zhongxiang Gui

Received: 19 March 2013 / Accepted: 1 October 2013 / Published online: 22 October 2013

Abstract Active gas melt laser cutting is the most commonly used method for phase hardened parts (PHP), because of the high strength of the material after hot stamping. In this article, the finite element analysis (FEA) and a series of experiments are carried out to predict temperature distribution, periodic striation, and microstructure evolution. Finally, a new sheet laser cutting modeling and active gas melt laser cutting heat source modeling are proposed, and they explain why periodic striation comes about; the optimal parameters for the lowest surface roughness are found; the microstructure distribution of the heat-affected zone (HAZ) is determined. It is found that there is a good correlation between the simulation and experimental results.

Keywords Active gas melt laser cutting · FEA · Temperature field · Periodic striation · HAZ · PHP

1 Introduction

In recent years, due to the demand for improvement in safety and the weight reduction of vehicles, the need to manufacture automobile structural components from ultra-high-strength hot-formed parts is apparent. In the hot stamping process [1] that is widely used to produce ultra-strength steel hot stamping parts used in cars, a quenchable boron blank is heated up to austenitizing temperature and baked for insulation in a furnace, immediately transferred to the press, and subsequently formed and quenched in the closed mold. After the hot press forming process, the formed and quenched parts often require subsequent processing such as blanking. The conventional mechanical blanking method is that the phase hardened parts (PHP) were trimmed by mold. However, due to the martensite microstructure and tensile strength (up to 1,500 MPa) of the PHP, the mechanical trimming mold was badly damaged, and the blanking edge cracked [2].

Currently, the active gas melt three-dimensional fiber laser cutting process is an important method to solve this problem. But, the periodic striation and surface roughness on the cross section was too large; tempering and re-austenization take place on the heat-affected zone of the trimming kerf.

Until now, a large number of research studies were carried out to study the laser cutting process. Finite element analysis (FEA) of the three-dimensional transient temperature field produced by laser beam scanning on the forming sheet is carried out by Zhong Ji et al. [3]. The Gaussian heat source model was used by Nyon et al. [4] to simulate the kerf width, temperature field, and thermal stress. A 2D analytical model that explained what caused the periodic striation was put forward by Lee Mein Wee et al. [5]. The process parameters for "free striation" with the condition of low gas pressure were researched by Lin Li et al. [6]. The phenomenon of "free striation" that was discovered in fiber laser cutting of low carbon steel was explained by Powell et al. [7]. An experimental advanced high-strength steel grade CP700 was cut to understand the effect of laser cutting process parameters on the formation of laser cut edges by Thomas [8].

However, few research studies have been focused on the active gas melt laser cutting of ultra-strength steel hot-stamped parts. And active gas melt laser cutting modeling and heat source modeling of sheet low carbon steel have not yet been determined; the reasons that caused striation and the size and microstructure of the heat-affected zone need to be studied. Experiments and FEA will be used to study the temperature field distribution, cutting cross-section surface morphology, surface roughness, and the size and microstructure of the heat-

P. Liu · Y. Zhang (✉) · H. Liu · Z. Gui
State Key Laboratory of Materials Processing and Die and Mould Technology, Huazhong University of Science and Technology, Wuhan 430074, China
e-mail: zhangys@mail.hust.edu.cn

Table 1 Percentage chemical composition of WH1300HF (weight percent)

C	Mn	Si	Cr	Al	P	B
0.2	1.3	0.25	0.18	0.02	0.005	0.002

affected zone in the different shape of the sheet and cutting process parameters.

2 Experimental

Experiments were performed to obtain the parameters of the laser cutting process and to validate the FEA model. The fiber laser (IPG YLR-400-MM-WC-Y11) delivering nominal output power of 400 W at multimode is used to irradiate the workpiece surface. The nominal focal length of the focusing lens is 127 mm (5″). A six-shaft hoisting robot (Stäubli RX160L) is used to control movement of the cutting head. Oxygen assisting gas emerging from the conical nozzle and coaxially with the laser beam is used.

In this experiment, the workpiece used is press hardened with WH1300HF sheet at 1.5 mm in thickness. The chemical composition of WH1300HF is given in Table 1. It is heated up to austenitizing temperature (950 °C) and baked for insulation in a furnace (5 min), immediately transferred to the press, and subsequently formed and quenched in the closed straight die. During the cutting process, two thermocouples (K-type) are jointed through spot weld around the kerf. They are connected to a data logger system (Self-development) to record the temperature history. Furthermore, the roughness value of the cross section is measured; surface morphology of the cross-section and microstructure of the heat-affected zone are analyzed through digital microscope (VHX-1000).

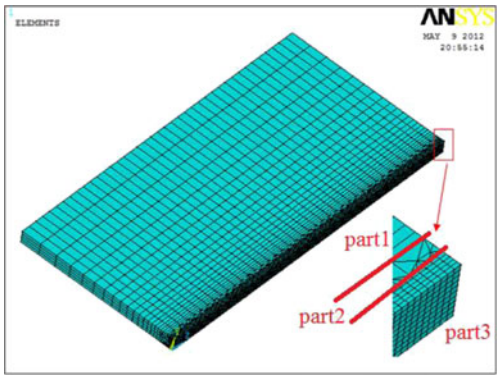

Fig. 2 Schematic view of the dimensions of the meshed coupon

3 Finite element analysis

3.1 Material parameters

Thermal–physical properties used in simulation are obtained from computer software JMatPro [9] as shown in Fig. 1. The properties are temperature dependent. Martensitic transformation and solid–liquid phase change are considered in the calculation. The melting point is 1,515 °C.

3.2 Finite element model

A nonuniform finite element (FE) mesh is used to save computational cost. Only half of the cutting workpiece is selected to be modeled by using the symmetry of the geometry and loads. As shown in Fig. 2, a dense mesh (SOLID90) is used in part 1 to obtain a good numerical accuracy, a much coarser mesh (SOLID70) is adopted for part 3, and a free mesh (SOLID87) is used for part 2 in order to connect the other two parts.

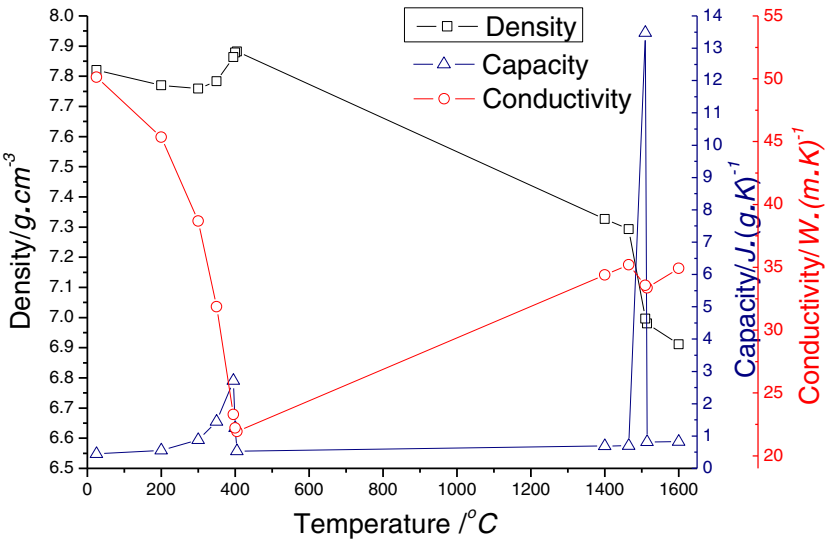

Fig. 1 Calculated thermal–physical properties of press-hardened WH1300HF steel

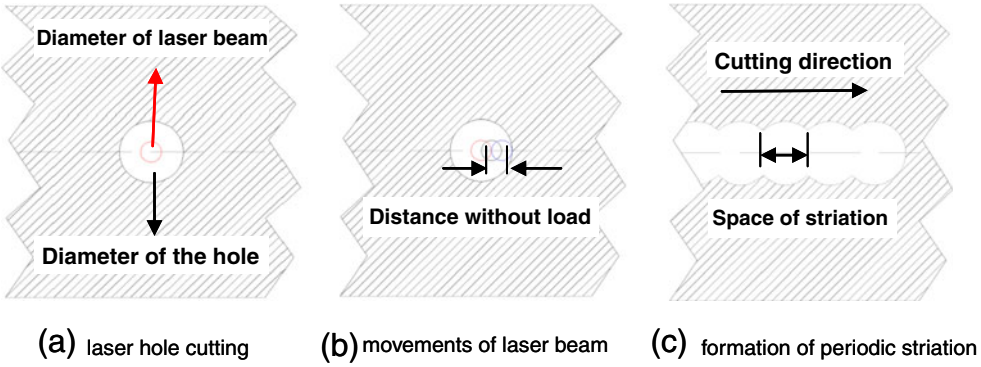

Fig. 3 Schematic diagram of sheet laser cutting modeling. **a** Laser hole cutting. **b** Movements of the laser beam. **c** Formation of periodic striation

3.3 Basic assumption

1. The cooling effect of the assist gas is ignored.
2. All the molten material is removed immediately from the workpiece by an assist gas. Thus, vaporization is negligible.
3. The entire workpiece is in the range of focal depth, so laser energy distribution in the thickness direction is the same.

3.4 Governing equation

The quasi-steady state temperature field in the laser cutting process is governed by the following equation:

$$\rho\frac{\partial(c_pT)}{\partial t}=\frac{\partial}{\partial x}\left(k\frac{\partial T}{\partial x}\right)+\frac{\partial}{\partial y}\left(k\frac{\partial T}{\partial y}\right)+\frac{\partial}{\partial z}\left(k\frac{\partial T}{\partial z}\right)+q_{\text{heat}}$$

where ρ is the density, c_p is the specific heat, and k is the thermal conductivity; they are all temperature dependent, as show in Fig. 2.

The boundary conditions for laser cutting are as follows:

At the symmetric plane, $\frac{\partial T}{\partial x}=0$

At the other surfaces, $-k\left(\frac{\partial T}{\partial n}\right)=\alpha_T(T-T_\infty)$

where T_∞ is the bulk temperature.

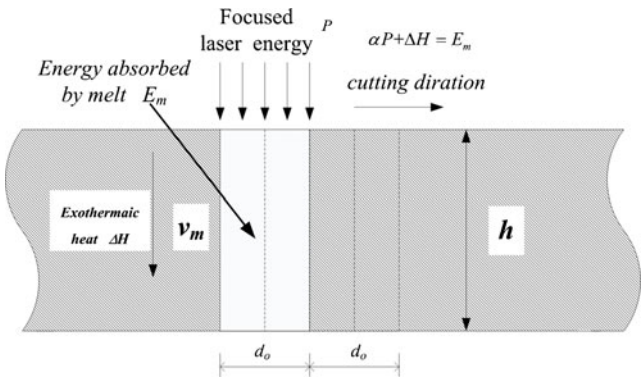

Fig. 4 Schematic diagram of the energy conservation

The combined heat transfer coefficient is as follows:

$$\alpha_T=\alpha_c+\alpha_r$$

where α_c is the convective heat transfer coefficient.

The radiation heat transfer coefficient is as follows [10, 11]:

$$\alpha_r=\varepsilon C_b\left[\left(\frac{T}{100}\right)^4-\left(\frac{T_\infty}{100}\right)^4\right]\frac{1}{T-T_\infty}$$

where ε is the blackness of the workpiece, and C_b is the blackbody radiation coefficient (5.67 $W/(m^2\cdot K^4)$).

3.5 Sheet laser cutting modeling

A new sheet laser cutting model is developed in this article, and a schematic diagram of the sheet laser cutting modeling is as shown in Fig. 3.

Laser cutting is mainly divided into three processes, as follows:

Firstly, laser hole cutting: under the action of the laser high-energy beam, the molten material is removed immediately from the workpiece by an assist gas, and then a circular hole formed; the diameter of the hole formed is greater than that of the laser beam due to thermal conductivity and oxidation combustion [12], as shown in Fig. 3a.

Secondly, movements of the laser beam: since the diameter of the beam is less than that of the molten material, the laser beam is not absorbed within a certain range, as shown Fig. 3b.

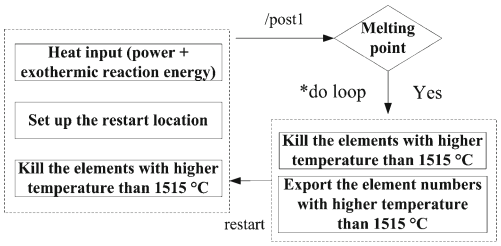

Fig. 5 Flow chart of the finite element simulation

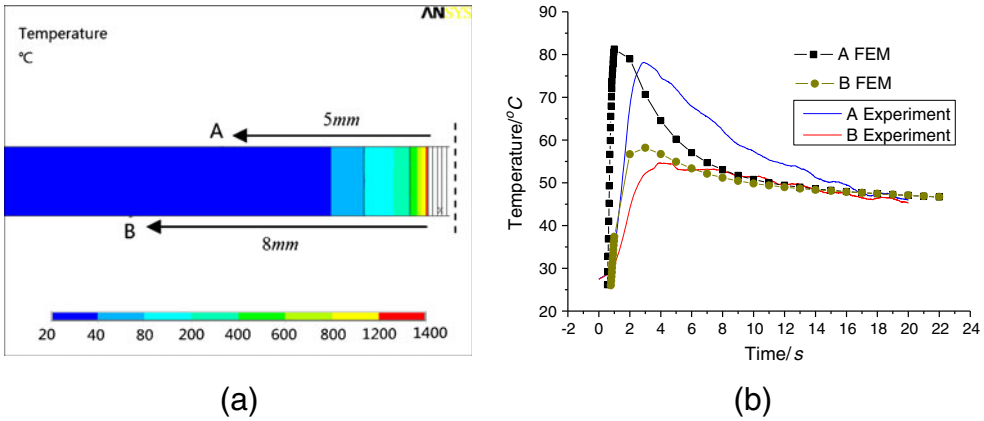

Fig. 6 **a** The numerically predicted cross-sectional views of laser cutting, **b** the comparison of numerically predicted and experimentally measured temperature. 400 W; 1.8 m/min; 0.6 MPa

Thirdly, formation of periodic striation: since the cutting speed is lower than the oxidation reaction speed, periodic striation formed [13, 14], and the formation of active gas melt laser cutting is as follows: heating–oxidation–subsidence–reoxidation–the formation of striation, as shown in Fig. 3c.

3.6 Sheet heat source modeling

More energy is released during the active gas melt laser cutting, for the chemical reaction. The main chemical reaction is as follows [15]:

$$\mathrm{Fe} + {}^{1}/_{2}\mathrm{O_2} = \mathrm{FeO} \quad \text{Condition : heating } \Delta H = -822 \text{ kJ mol}^{-1}$$

According to energy conservation, an analytical model for vertical melting speed (v_m) is developed during the active gas melt laser cutting. As shown in Fig. 4, the equation of the energy required to convert a mass m of a material in a cubic element at room temperature into a melt is the following [16]:

$$E_m = m \cdot \Delta E$$

where E_m is the energy required to melt the material, ΔE is the enthalpy change per unit mass of solid–liquid transition. We then use the following equation:

A mass m is as follows:

$$m = \rho V = \rho \frac{\pi d_o^2}{4} h = \rho \frac{\pi d_o^2}{4} v_m \cdot t$$

The equation of energy conservation is as follows:

$$E_m / t = \alpha \cdot P + \Delta H$$

where α is the absorptive index, ΔH is the exothermic reaction energy.

Since the energy conservation, the vertical melting speed (v_m) is determined as follows:

$$v_m = \frac{4(\alpha P + \Delta H)}{\pi \Delta E \rho d_o^2} \approx 4 m/s$$

Since the analytical solution of the vertical melting speed v_m is about 4 m/s, so that is far greater than cutting speed.

A new sheet heat source modeling for active gas melt laser cutting is developed in this research. The new volume heat source expressed follows:

$$S_o(x,y,z) = I_o e^{\left(-\left(x^2+y^2\right)/r^2\right)} + \frac{\Delta H}{\left(h \cdot \pi d_o^2/4\right)} \quad ; \quad I_o = \frac{\alpha P}{\left(h \cdot \pi d_o^2/4\right)}$$

where r is the radius of the laser beam, I_o is the real energy density.

3.7 Technical route

A flow chart of the finite element simulation is presented in Fig. 5. An APDL-based subroutine is written to simulate the

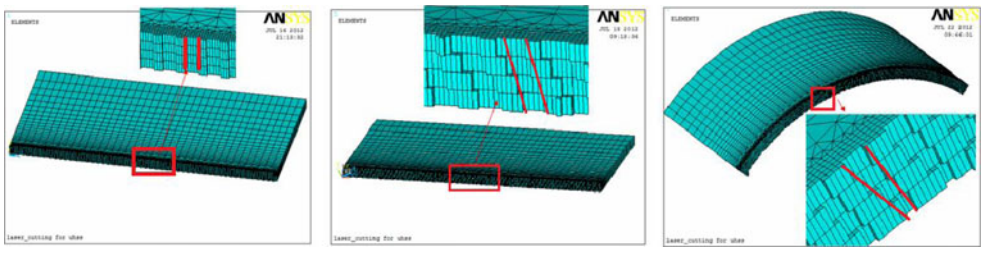

Fig. 7 Three kinds of numerically predicted surface appearance (400 W; 1.8 m/min; 0.6 MPa)

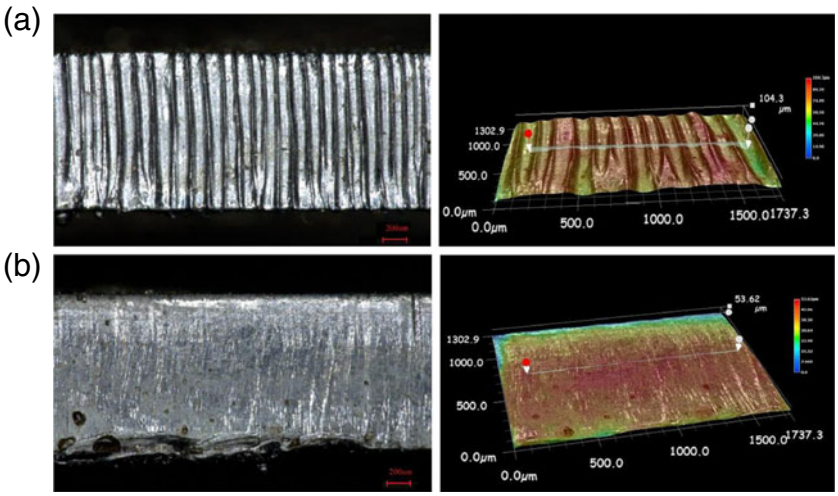

Fig. 8 The experimentally measured surface appearance **a** with distinct striation at 1.8 m/min cutting speed and **b** with nondistinct striation at 3 m/min cutting speed

melting areas of the metal. From the temperature distribution profile, the elements at which temperature is greater than the melting point (1,515 °C) of the WH1300HF steel are killed. The restart function is used to continue the analyses, for the elements with higher temperature than the melting point should be found via the post processing in any do loop.

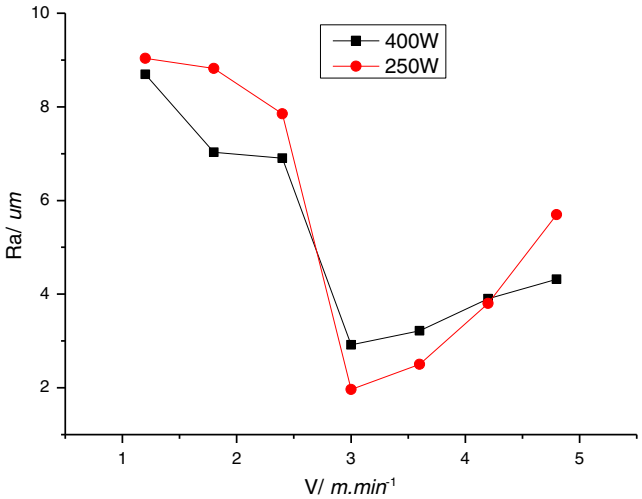

Fig. 9 The variation of surface roughness with cutting speeds under different laser powers

4 Results and discussions

4.1 Temperature field

The numerically predicted cross-sectional view of laser cutting is shown in Fig. 6a, which also shows the position of the two thermocouples in the workpiece (A and B). Figure 6b shows the comparison of the numerically modeled temperature distribution with respect to the measured temperature by thermocouples. It is shown that there is a good agreement between the numerically predicted and experimentally measured results.

4.2 Surface appearance

Three kinds of numerically predicted surface appearance that are taken from post processing by unkilled elements are shown in Fig. 7. The experimentally measured surface appearance with distinct striation at the condition of $\delta = 90°$ is shown

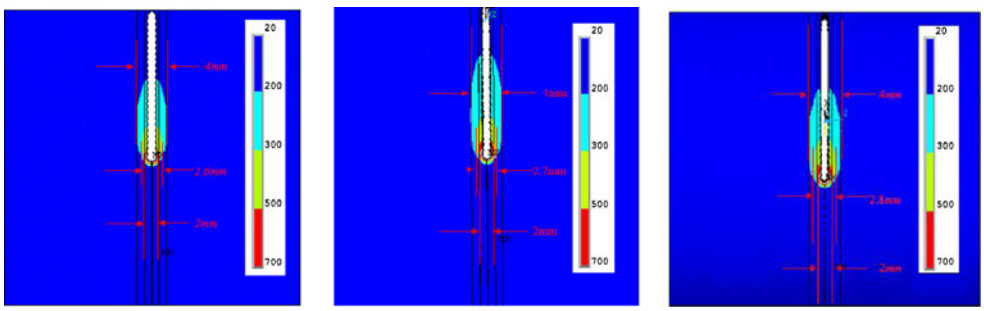

Fig. 10 Numerically predicted heat transfer distribution at the top surface

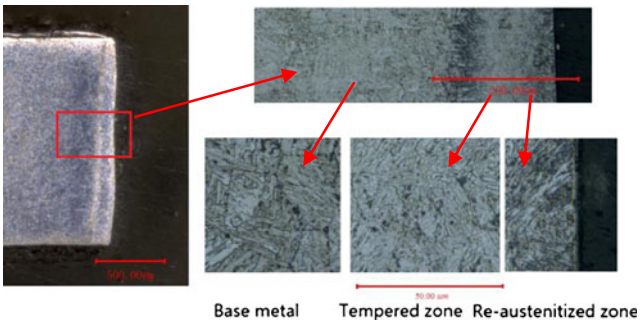

Fig. 11 Microstructure of HAZ

in Fig. 8a. It is shown that there is a good agreement between the numerically predicted and experimentally measured results.

The variation of surface roughness with cutting speeds under different laser powers (250 and 400 W) is shown in Fig. 9. These results show that surface roughness decreases as the cutting speed increases until an optimal speed is reached; beyond which surface roughness gradually increases again.

4.3 Characterizations of HAZ

Figure 10 shows numerically predicted heat transfer distribution at the top surface. The size of the HAZ in the different shape of the sheet and cutting process parameters is the same (200, 300, and 500 °C as monitoring points).

The experimentally measured microstructure of HAZ is shown in Fig. 11. The HAZ is divided into three main regions: re-austenitized zone, tempered zone, and base metal. Figure 6a shows the temperature distribution on the cross section, and the isothermal line is parallel. It is evident that there is a good agreement between these two kinds of results.

5 Conclusions

An experimentally based thermal FE model, where a new sheet laser cutting modeling and active gas melt laser cutting heat source modeling are proposed, could be used to predict the temperature field, surface appearance, and size of the HAZ in the different shape of the sheet and cutting process parameters.

The reason why the periodic striation comes about is explained. The optimal process parameters for the lowest surface roughness under different laser powers (250 and 400 W) are found.

The microstructure distribution of the HAZ is determined and shows that three main regions (re-austenitized zone, tempered zone, and base metal) are found. These results can provide a reference for the three-dimensional optical fiber laser trimming process of the actual PHP.

Acknowledgments This study was supported by the National Basic Research Program of China ("973" Program) (grant no. 2010CB630803) and the National Natural Science Foundation of China (grant no. 51275185).

References

1. Karbasian H, Tekkaya AE (2010) A review on hot stamping. J Mater Process Technol 210:2103–2118
2. So H, Faßmann D, Hoffmann H, Golle R, Schaper M (2012) An investigation of the blanking process of the quenchable boron alloyed steel 22MnB5 before and after hot stamping process. J Mater Process Technol 212:437–449
3. Ji Z, Shichun W (1998) FEM simulation of the temperature field during the laser forming of sheet metal. J Mater Process Technol 74: 89–95
4. Nyon K, Nyeoh C, Mokhtar M, Abdul-Rahman R (2012) Finite element analysis of laser inert gas cutting on Inconel 718. Int J Adv Manuf Technol 60:995–1007
5. Wee LM, Li L (2005) An analytical model for striation formation in laser cutting. Appl Surf Sci 247:277–284
6. Li L, Sobih M, Crouse PL (2007) Striation-free laser cutting of mild steel sheets. CIRP Annals - Manuf Techn 56:193–196
7. Powell J, Al-Mashikhi SO, Kaplan AFH, Voisey KT (2011) Fibre laser cutting of thin section mild steel: an explanation of the 'striation free' effect. Opt Laser Eng 49:1069–1075
8. Thomas DJ (2013) The effect of laser cutting parameters on the formability of complex phase steel. Int J Adv Manuf Technol 64: 1297–1311
9. Guo Z, Saunders N, Schillé JP, Miodownik AP (2009) Material properties for process simulation. Mat Sci Eng A 499:7–13
10. von Böckh P, Wetzel T (2012) Heat transfer: basics and practice. Springer, Berlin, pp 189–196
11. Chao W, YiSheng Z, XiaoWei T, Bin Z, Jian L (2012) Thermal contact conductance estimation and experimental validation in hot stamping process. Sci China Technol Sc 55:1852–1857
12. Yilbas BS, Akhtar SS, Karatas C (2012) Laser hole cutting into Ti-6Al-4V alloy and thermal stress analysis. Int J Adv Manuf Technol 59:997–1008
13. Arata Y, Hiroshi MARUO, Isamu MIYAMOTO, Sadao TAKEUCHI (1979) Dynamic behavior in laser gas cutting of mild steel. Trans JWRI 8:175–186
14. Di Pietro P, Yao YL (1994) An investigation into characterizing and optimizing laser cutting quality—a review. Int J Mach Tools Manu 34:225–243
15. Ion JC (2005) Laser processing of engineering materials. Elsevier, Amsterdam, pp 347–350
16. Radovanović M (2006) Some possibilities for determining cutting data when using laser cutting. J Mech Eng 52:645–652